

QASA: Quality-Guided K-Adaptive Slot Attention for Unsupervised Object-Centric Learning

Tianran Ouyang¹, Xingping Dong^{1*}, Jing Zhang², Mang Ye¹, Jun Chen¹, Bo Du¹

¹Wuhan University

²Australian National University

Abstract

*Slot Attention, an approach that binds different objects in a scene to a set of "slots", has become a leading method in unsupervised object-centric learning. Most methods assume a fixed slot count K , and to better accommodate the dynamic nature of object cardinality, a few works have explored K -adaptive variants. However, existing K -adaptive methods still suffer from two limitations. First, they do not explicitly constrain slot-binding quality, so low-quality slots lead to ambiguous feature attribution. Second, adding a slot-count penalty to the reconstruction objective creates conflicting optimization goals between reducing the number of active slots and maintaining reconstruction fidelity. As a result, they still lag significantly behind strong K -fixed baselines. To address these challenges, we propose **Quality-Guided K-Adaptive Slot Attention (QASA)**. First, we decouple slot selection from reconstruction, eliminating the mutual constraints between the two objectives. Then, we propose an unsupervised Slot-Quality metric to assess per-slot quality, providing a principled signal for fine-grained slot-object binding. Based on this metric, we design a Quality-Guided Slot Selection scheme that dynamically selects a subset of high-quality slots and feeds them into our newly designed gated decoder for reconstruction during training. At inference, token-wise competition on slot attention yields a K -adaptive outcome. Experiments show that QASA substantially outperforms existing K -adaptive methods on both real and synthetic datasets. Moreover, on real-world datasets QASA surpasses K -fixed methods.*

1. Introduction

Object-centric learning (OCL) seeks to decompose scenes into sets of object representations that align with the causal structure of the physical world. Because scenes are compositional, such representations tend to be more robust to distribution shifts [6] and facilitate downstream tasks such as reasoning and control [1, 2, 23, 29]. Motivated by the

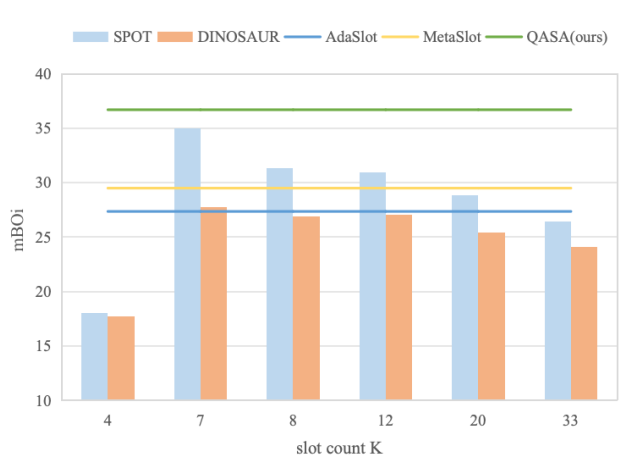


Figure 1. **mBOi vs. slot count K on COCO [20]**. K -fixed methods (e.g., SPOT [16], DINOSAUR [24]) exhibit large performance fluctuations as K varies. By contrast, K -adaptive methods do not require searching for the best K . Our method QASA substantially outperforms existing K -adaptive baselines (MetaSlot [21], AdaSlot [12]) and even surpasses strong K -fixed baselines.

abundance of unlabeled images, we focus on *unsupervised object-centric learning*, where models learn object-centric representations directly from visual data. Most unsupervised OCL approaches rely on reconstruction objectives combined with set-structured bottlenecks that map an image to a small set of "slots", which are then decoded back to the input space [22]. Within this line of work, Slot Attention has emerged as a mainstream approach [12, 24, 26, 27, 31].

In different images, the number of objects varies dynamically, and thus the slot count K should vary accordingly. However, most methods fix the slot count K a priori, making object-slot mismatches inevitable. As shown in Fig. 1, the model's performance is highly sensitive to the choice of K . To obtain a suitable value of K , one often has to expend substantial resources on per-dataset tuning. Even then, the contradiction between a fixed K and dynamically varying object counts remains. A pioneering K -adaptive approach, AdaSlot [12], trains a slot selector by adding a slot-

*Corresponding author.

count penalty to the training objective. However, the reconstruction objective tends to use more slots, which conflicts with the slot-count penalty. Other lines of work perform slot selection via principal component analysis (CoSA [18]) or by maintaining a unified slot codebook (MetaSlot [21]). However, all these methods directly or indirectly rely on the prominence of object features, and thus tend to select only the most prominent objects for binding. This reliance on prominence leads to ambiguous slot–object attribution, where slots fail to bind precisely to specific objects and instead capture only coarse trends. Empirically, existing K -adaptive methods lag far behind K -fixed baselines, particularly in real-world scenarios. These issues hinder the practical adoption of K -adaptive Slot Attention.

To address these challenges, we propose **Quality-Guided K -Adaptive Slot Attention (QASA)**. Unlike prior approaches that train a small auxiliary network to select slots during reconstruction, QASA decouples slot selection from reconstruction. To select high-quality slots under unsupervised conditions, we introduce a novel Slot-Quality metric. Inspired by the competitive token assignment in Slot Attention [22, 24], we define slot’s quality as the proportion of its attention mass within its winning region. Ideally, a high-quality slot wins entirely on its own tokens and assigns negligible mass elsewhere. Building on this metric, we propose a Quality-Guided Slot Selection scheme that, for each image, iteratively adds the highest-quality slots to a qualified set until a coverage threshold is met. We feed the slots into gated decoders, using gating to suppress the contributions of unselected slots, and compute the reconstruction loss. We evaluate QASA on real-world datasets (COCO [20], PASCAL VOC [11]) and synthetic datasets (MOVi-C/E [14]). QASA substantially outperforms existing K -adaptive methods. Furthermore, relative to K -fixed methods, it achieves state-of-the-art performance on real-world data. Our key contributions are as follows:

- We introduce a novel unsupervised **Slot-Quality** metric, defined as the proportion of its attention mass within its winning region, providing an effective signal to guide precise slot–object binding.
- We propose a **Quality-Guided Slot Selection** module that jointly leverages quality, coverage, and novelty to guide the model to focus only on the most matching slot subset for each image.
- We design **gated Transformer** and **gated MLP** decoders. Under both types of decoders, our method surpasses existing approaches, demonstrating the high compatibility of our proposed quality-guided mechanism.
- Across real and synthetic datasets, our method markedly outperforms existing K -adaptive baselines by **8.4%** on average, and achieves **state-of-the-art** results vs. K -fixed methods on real data.

2. Related work

Object-Centric Learning. Object-centric learning (OCL) represents scenes as compositions of discrete objects. Early approaches fall into two families: spatial-attention models that infer object bounding boxes [5, 10, 19] and scene-mixture models trained with variational inference [3, 8, 13]. Slot Attention [22] crystallizes a set-structured bottleneck by iteratively assigning features to a fixed set of latent slots and has become a mainstream paradigm in recent years. *Building on Slot Attention*, a variety of improvements have been proposed, roughly falling into four threads: (i) *reconstruction target*: DINOSAUR [24] reconstructs pre-trained features instead of pixels to better scale to real images; (ii) *decoders*: SLATE [25] conditions an autoregressive/quantized decoder on slots to enhance detail and compositionality, and diffusion-based decoders further improve fidelity (e.g., Latent Slot Diffusion (LSD) [15] and SlotDiffusion [28]); (iii) *training strategy*: SPOT [16] leverages self-training with a patch-order permutation to strengthen slot pipelines on real images; (iv) *video*: SAVi/SAVi++ [7, 17] extend slot attention to videos with weak cues or depth targets, and VideoSAUR [30] exploits temporal feature similarity for real-world sequences. However, these advances still assume a pre-specified slot count K . When K mismatches scene complexity, under- and over-segmentation and wasted capacity occur, hampering learning and transfer [12]. We therefore treat K as *per-image adaptive*, retaining an image-specific set of slots.

K -Adaptive Slot Attention. K -Adaptive Slot Attention aims to match model capacity to scene complexity rather than fixing K globally. A representative selection-based approach is AdaSlot [12], which starts from a large K_{\max} and learns a lightweight selector with expected- K regularization plus a masked decoder to keep only informative slots. A complementary direction estimates K via prototypes: CoSA learns a grounded slot dictionary and uses a spectral criterion to activate the needed slots, reducing redundancy [18]. MetaSlot further maintains a codebook and prunes duplicate slots by vector-quantizing slot embeddings before refinement, thereby adapting K and improving efficiency [21]. Outside the Slot Attention family, GENESIS-V2 employs a stochastic stick-breaking prior to infer a variable number of components in a generative framework [9]. Despite clear progress, existing K -adaptive designs tend to favor *prominent* objects over fine structures and are commonly coupled with MLP-style decoders, complicating integration with stronger Transformer decoders. In contrast, we introduce a *slot-quality* criterion to select and retain high-quality slots with fine-grained details. It is decoder-agnostic, supporting both MLP and Transformer decoders. This yields substantial gains and surpasses strong K -fixed baselines on complex scenes.

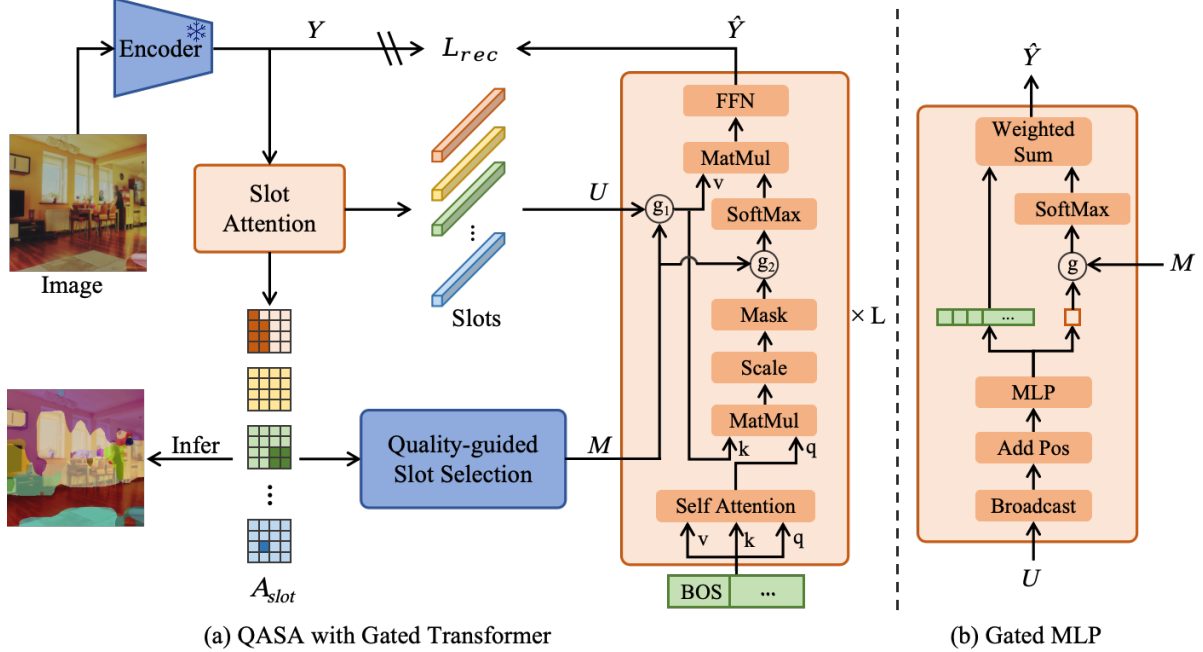


Figure 2. **Framework of Quality-Guided K -Adaptive Slot Attention (QASA).** The overall training pipeline follows the canonical Slot Attention architecture: an image is encoded by the encoder, fed into the Slot Attention module, and then decoded; the reconstruction loss is computed against embeddings produced by a *frozen* encoder. The key difference is that we compute a slot-quality metric from the Slot Attention maps A^{slot} and use it to select a subset of slots, allowing only the selected slots to participate in decoding. At inference, no slot selection is applied. Instead, all slots compete, based on A^{slot} , for each token to produce a K -adaptive result.

3. Method

3.1. Overview

Slot Attention typically comprises three parts: *encoder*, *slot-attention* and *decoder*. First, an encoder extracts N patch-wise features $Y \in \mathbb{R}^{N \times d_y}$ from an input image X . Then, a slot-attention module groups these features into K latent vectors $U = (u_1, \dots, u_K) \in \mathbb{R}^{K \times d_u}$, referred to as *slots*, each intended to represent one object in the image. Finally, a decoder reconstructs a target signal, either the original image X or the features Y , from these slots. Slot Attention is commonly evaluated using attention masks A that indicate the association of each image patch with a specific slot. These masks can be obtained either from the slot-attention module or from the decoder, denoted A^{slot} and A^{dec} , respectively. In this paper, we consistently use masks A^{slot} from the slot-attention module for evaluation.

Prior K -adaptive method AdaSlot [12] tackles the fixed- K issue in Slot Attention by using a lightweight selector to mask slots and adding an expected- K regularizer. However, reconstruction favors using more slots and conflicts with the slot-count penalty, so joint training often yields unstable or ambiguous bindings. In contrast, CoSA [18] separates slot selection via a PCA-based criterion, and MetaSlot [21] maintains a global codebook to quantize and prune redundant slots. Yet these approaches either emphasize reducing slot count or pick slots by the prominence of principal components, without defining the desired properties of the retained slots, which should capture *fine-grained, object-specific structure* with attention confined to the target. We instead introduce an unsupervised *Slot-Quality* metric that evaluates whether a slot binds *fine-grained target features* rather than broad, diffuse representations, explicitly favoring concentration within the object. Building on this metric, we introduce **Quality-Guided K -Adaptive Slot Attention (QASA)**, which selects slots through a metric-based procedure, thereby avoiding the contradiction introduced by slot-count regularization. As shown in Fig. 2(a), QASA consists of four parts: *encoder*, *slot-attention*, *slot selection* and *gated decoder*.

During training, we set a maximum slot count K_{\max} , and we select an appropriate set of slots according to A^{slot} (detailed in § 3.2) as $M = F_{\text{select}}(A^{\text{slot}})$. Then we feed the slots together with the selection mask into our proposed gated decoder (detailed in §. 3.3), obtaining $\hat{Y} = \text{Dec}_{\text{gated}}(U, M)$. Following DINOSAUR [24] and SPOT [16], we use DINO [4] as the image encoder and reconstruct its features $\hat{Y} \in \mathbb{R}^{N \times d_y}$ as the training target. The model is trained with the reconstruction loss: $\mathcal{L}_{\text{rec}} = \frac{1}{N \cdot d_y} \|Y - \hat{Y}\|_2^2$.

During inference, no slot selection is applied and *all* slots compete, based on A^{slot} , for each token to produce a K -adaptive result. Concretely, for each patch $y_t \in Y$ we take a hard winner over the slot-attention map A^{slot} via $w_t = \text{argmax}_{i \in \{1, \dots, K_{\max}\}} A_{t,i}^{\text{slot}}$, and assign patch y_t to the slot with the strongest association, i.e., y_t is assigned to slot w_t . This induces a hard partition of tokens, $\mathcal{S}_i = \{t \mid w_t = i\}$, and we treat the union of patches indexed by \mathcal{S}_i as the region assigned to slot i . Since the slot-attention masks are defined on the encoder’s token grid (low resolution), we upsample them to the original image resolution before evaluating against ground-truth masks.

3.2. Quality-Guided Slot Selection

To perform training-free slot selection, the central challenge is to evaluate the quality of the slots in an unsupervised setting. The attention map of the slot-attention module A^{slot} provides an excellent signal. Ideally, the attention of a high-quality slot A_i^{slot} would be 1 over its object region and 0 elsewhere, but in the unsupervised setting the object regions are unknown. Inspired by Slot Attention’s competitive assignment mechanism, in which attention maps induce competition among slots for responsibility over all tokens, we propose a competition-based slot-quality metric.

Let $A \in [0, 1]^{N \times K_{\max}}$ denote the slot-attention probabilities for all tokens (patches) and slots, normalized over slots (i.e., $\sum_{i=1}^{K_{\max}} A_{t,i} = 1$ for each token t). For each token t , define its winner slot:

$$w_t = \text{argmax}_{i \in \{1, \dots, K_{\max}\}} A_{t,i}. \quad (1)$$

For slot i , define the winner mass and total mass:

$$W_i^{\text{win}} = \sum_{t: w_t=i} A_{t,i}, \quad W_i = \sum_{t=1}^N A_{t,i}. \quad (2)$$

The slot-quality score is

$$Q_i = \frac{W_i^{\text{win}}}{W_i + \epsilon} \in [0, 1], \quad (3)$$

which measures the purity of $slot_i$ ’s mass within the region where it wins.

Based on *slot-quality*, we propose a Quality-Guided Slot Selection scheme that also considers *coverage*, as detailed in Algorithm 1. We set a *per-token coverage-quality threshold* $\tau \in (0, 1]$ and a *coverage-rate threshold* $\rho \in (0, 1]$. A token t is marked as *covered* if the cumulative attention mass from the selected slots $S \subseteq \{1, \dots, K_{\max}\}$ exceeds τ :

$$\text{Covered}_S(t) = \mathbb{1} \left[\sum_{i \in S} A_{t,i} \geq \tau \right]. \quad (4)$$

The overall coverage rate is then

$$\text{Coverage}(S) = \frac{1}{N} \sum_{t=1}^N \text{Covered}_S(t). \quad (5)$$

Algorithm 1 Quality-Guided Slot Selection

Input: Slot-attention probabilities $A \in [0, 1]^{N \times K_{\max}}$, thresholds τ, ρ, μ .
Output: Selection mask $M \in \{0, 1\}^{K_{\max}}$.

- 1: **Compute qualities:** obtain Q using Eq. 3 (with w_t from Eq. 1 and W_i^{win}, W_i from Eq. 2).
- 2: $S \leftarrow \emptyset, M \leftarrow \mathbf{0}_{K_{\max}}$.
- 3: $\pi \leftarrow \text{argsort}_{i \in \{1, \dots, K_{\max}\}} (-Q_i)$ \triangleright indices in descending Q
- 4: **for** $j = 1$ to K_{\max} **do**
- 5: $i \leftarrow \pi_j$.
- 6: **if** $\text{novelty}(i \mid S)$ from Eq. 6 $< \mu$ **then continue**
- 7: **end if**
- 8: $S \leftarrow S \cup \{i\}$.
- 9: **if** $\text{Coverage}(S)$ from Eq. 5 (with Covered_S from Eq. 4) $\geq \rho$ **then**
- 10: **break**
- 11: **end if**
- 12: **end for**
- 13: Set $M_i \leftarrow 1$ for all $i \in S$; **return** M .

We greedily add slots in descending order of quality Q_i 3 until $\text{Coverage}(S) \geq \rho$. To avoid repeatedly selecting slots that mostly explain already-covered regions, we enforce a *novelty constraint*: a candidate slot i is skipped if the fraction of its mass on already-covered tokens exceeds a threshold. Writing $C_S = \{t \mid \text{Covered}_S(t) = 1\}$ for the current covered set, the novelty of slot i w.r.t. S is

$$\text{novelty}(i \mid S) = 1 - \frac{\sum_{t \in C_S} A_{t,i}}{\sum_{t=1}^n A_{t,i} + \epsilon}. \quad (6)$$

We accept i only if $\text{novelty}(i \mid S) \geq \mu$ with $\mu \in [0, 1)$. The resulting mask M is used during training; no mask is applied at inference.

3.3. Gated Decoder

After completing slot selection, we need to remove the influence of unselected slots during decoding. A straightforward approach is to dynamically gate all slots according to the mask, suppressing the contribution of unselected slots during decoding. For a fair comparison, we simply augment the MLP [24] and Transformer [16] decoders used in prior K -fixed methods with our gating mechanism, without introducing any additional network components.

Gated Transformer Decoder. We adapt the standard Transformer decoder architecture [16] by introducing a dual gating mechanism into its cross-attention layers, as illustrated in Fig. 2(a). This mechanism leverages the selection mask $M \in \{0, 1\}^{K_{\max}}$ from our quality-guided selection process (Algorithm 1) to create two distinct gates for fine-grained control over slot participation.

Given the selection mask M , we define a hard K/V gate $g_1 \in \{\varepsilon_1, 1\}_{\max}^K$ and a soft logits gate $g_2 \in \{\varepsilon_2, 1\}_{\max}^K$, where $0 < \varepsilon_1, \varepsilon_2 < 1$. For each slot $i \in \{1, \dots, K_{\max}\}$, the gates are defined as

$$(g_1)_i = M_i + (1 - M_i)\varepsilon_1, \quad (g_2)_i = M_i + (1 - M_i)\varepsilon_2. \quad (7)$$

Within each cross-attention block, the attention mechanism is modified as follows. First, the key (K) and value (V) vectors from the slots are multiplicatively modulated by the hard gate g_1 to physically suppress the information flow from unselected slots. Second, an additive bias based on the soft gate g_2 is applied to the attention logits before the softmax operation. This penalizes the scores of unselected slots, ensuring they do not win the attention competition. The full gated attention output is computed as:

$$\text{Output} = \text{softmax} \left(\frac{Q(K \odot g_1)^\top}{\sqrt{d_k}} + \log(g_2) \right) (V \odot g_1), \quad (8)$$

where \odot denotes the element-wise product broadcasted across the feature dimension. This dual mechanism ensures that unselected slots are robustly pruned from both the information pathway (via g_1) and the competitive attention allocation (via g_2).

Gated MLP Decoder. The MLP decoder predicts per-slot reconstructions $\{\hat{y}_{i,t} \in \mathbb{R}^d\}_{i=1}^{K_{\max}}$ for tokens $t = 1, \dots, N$ together with mixture logits $\ell \in \mathbb{R}^{K_{\max} \times N}$ over the slot dimension. Given a binary selection mask $M \in \{0, 1\}^{K_{\max}}$ (active set $S = \{i \mid M_i = 1\}$), we apply hard gating at the logit level, as shown in Fig. 2(b), and then normalize only over active slots:

$$\ell'_{i,t} = \begin{cases} \ell_{i,t}, & M_i = 1, \\ -\infty, & M_i = 0, \end{cases} \quad (9)$$

where $i \in \{1, \dots, K_{\max}\}$, $t \in \{1, \dots, N\}$.

$$\alpha_{i,t} = \frac{\exp(\ell'_{i,t})}{\sum_{j=1}^{K_{\max}} \exp(\ell'_{j,t})} = \frac{M_i \exp(\ell_{i,t})}{\sum_{j=1}^{K_{\max}} M_j \exp(\ell_{j,t})}, \quad (10)$$

The final reconstruction aggregates per-slot predictions using the gated mixture:

$$\hat{y}_t = \sum_{i=1}^{K_{\max}} \alpha_{i,t} \hat{y}_{i,t}, \quad t \in \{1, \dots, N\}. \quad (11)$$

The masks reported for evaluation are $\alpha \in [0, 1]^{K_{\max} \times N}$ reshaped to the token grid. In practice, we implement the $-\infty$ gate by filling inactive-slot logits with a large negative constant $-\mathcal{C}$ (with $\mathcal{C} \gg 0$) before the softmax. Equivalently, $\ell'_{i,t} = \ell_{i,t} - (1 - M_i)\mathcal{C}$. We ensure $|S| \geq 1$.

4. Experiments

4.1. Setup

We evaluate on two widely used real-world datasets, **MS COCO 2017** [20] and **PASCAL VOC 2012** [11], and two synthetic datasets, **MOVi-C** and **MOVi-E** [14]. Our emphasis is on real-world scenes: COCO contains diverse, cluttered images with many co-occurring objects and is notably challenging, whereas VOC typically features one or a few salient objects and serves as a complementary regime. For synthetic evaluation, MOVi provides rendered scenes with high-quality 3D-scanned assets. MOVi-C has 3–10 objects per scene and MOVi-E has 11–23. Following prior work [24], we treat MOVi videos as image datasets by sampling random frames.

Metrics. Following recent work [12, 16, 24, 27], we report Mean Best Overlap (mBO) at the instance (mBOi) and class (mBOc) levels. For mBO, each ground-truth mask is paired with the single predicted mask that maximizes IoU, allowing many-to-one matches, and scores are then averaged per instance (mBOi) or per class (mBOc). We also report mean Intersection over Union (mIoU) under a stricter one-to-one protocol, where predicted and ground-truth masks are matched with the Hungarian algorithm before averaging. In line with [27], we do not report FG-ARI, since it ignores background regions and is insensitive to boundary quality, which can yield misleadingly optimistic segmentation scores [16].

Implementation Details. Unless otherwise specified, all settings follow SPOT [16]. For all datasets, we set $\rho = 0.8$ and $\mu = 0.3$. For COCO and VOC, we set $\tau = 0.5$. And for MOVi, we set $\tau = 0.8$. For COCO and VOC, we set K_{\max} to the maximum number of masks plus one (to include background), i.e., $K_{\max} = 33$ and $K_{\max} = 20$, respectively.* For MOVi-C and MOVi-E, we round the maximum mask count up to the nearest multiple of ten and use $K = 20$ and $K = 30$, respectively. We use 4× RTX 4090 GPUs for COCO and 2× RTX 4090 GPUs for the other datasets. With the Transformer decoder, the per-GPU batch size is 256. With the MLP decoder, the per-GPU batch size is 32. We train for 100 epochs on COCO and MOVi, and for 600 epochs on PASCAL VOC. For training stability, we adopt a warm-up strategy in which all slots participate in reconstruction in the early epochs. With the Gated Transformer decoder, we set $warmup_{gate} = 10$ on VOC and 20 on MOVi-C/E. With the Gated MLP decoder, we set $warmup_{gate} = 10$ on VOC, 10 on MOVi-C, and 5 on MOVi-E. On COCO, we disable this warm-up (i.e., $warmup_{gate} = 0$). Detailed experimental settings are provided in the supplementary material.

*In the VOC training set, apart from a single sample with 38 masks, all others have at most 19 masks, so we ignore this outlier.

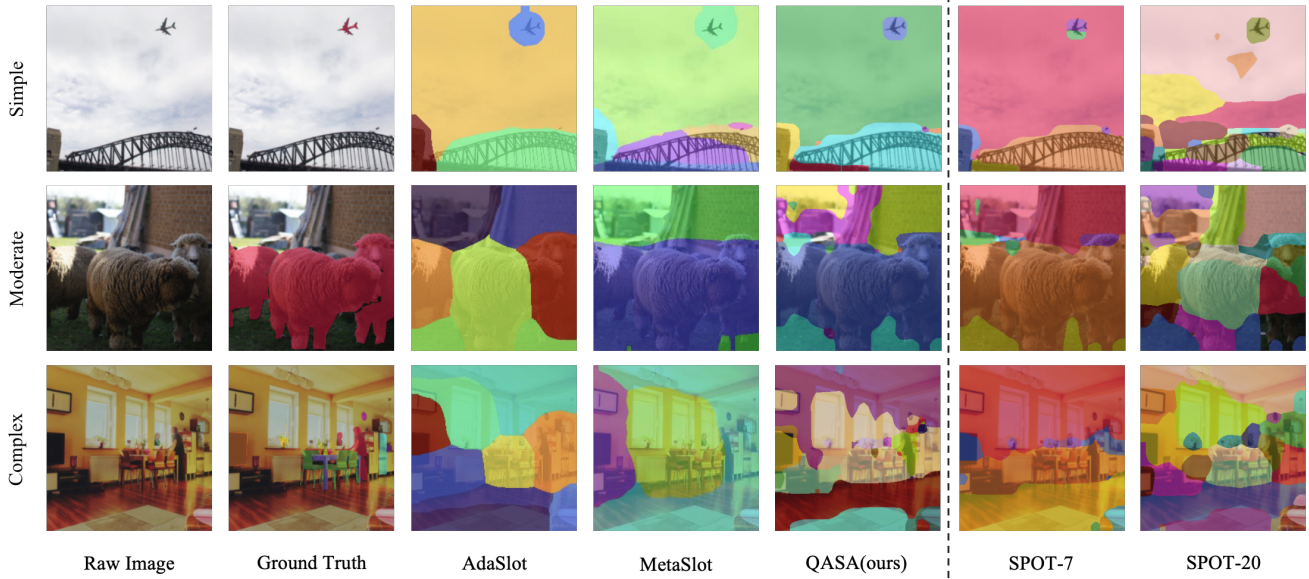


Figure 3. **Visualizations on COCO.** The AdaSlot examples are taken from its original paper [12]. The MetaSlot examples are generated using the authors’ released checkpoint [21]. “SPOT-7” and “SPOT-20” denote SPOT [16] with $K = 7$ and $K = 20$, respectively. The SPOT-7 examples are generated using the authors’ released checkpoint. The SPOT-20 examples are generated by training a model under the same settings as in the original paper.

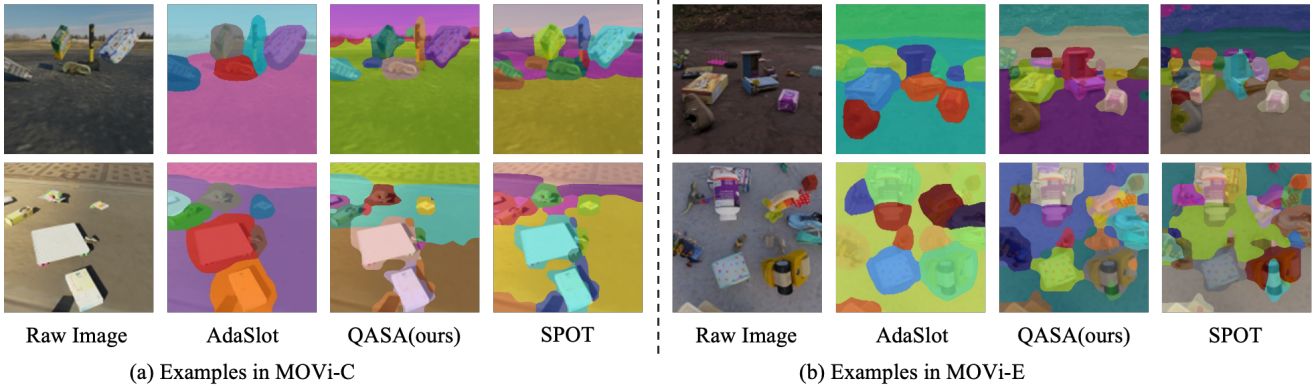


Figure 4. **Visualizations on MOVi-C/E.** The AdaSlot examples are taken from its original paper [12]. the SPOT examples are generated by training a model under the same settings as in the original paper. MetaSlot has not released code for MOVi-C/E, so these results are not included in our comparison.

4.2. Main Results

Comparison with K -adaptive methods. To the best of our knowledge, AdaSlot [12], CoSA [18], and MetaSlot [21] are the only three K -adaptive Slot Attention methods to date. Because CoSA lacks publicly available experimental artifacts for comparison, we report results against AdaSlot and MetaSlot only. As shown in Tab. 2, our method QASA outperforms AdaSlot and MetaSlot by a large margin on both real-world (COCO) and synthetic (MOVi) datasets, with an average improvement of **8.4%** in mBOi. Even when using an MLP decoder to match

their setup, QASA-MLP still surpasses them substantially, achieving a **4.7%** gain in mBOi. We present visualizations stratified by scene complexity to intuitively demonstrate the advantages of QASA on COCO, as shown in Fig. 3. It is clear that QASA outperforms AdaSlot [12] and MetaSlot [21] across all three levels (simple, moderate, and complex). QASA adapts to varying object counts and captures fine-grained object details, whereas AdaSlot largely partitions images into coarse blob-like regions. This issue is especially pronounced in complex scenes. MetaSlot can capture certain fine details, but its performance degrades markedly in complex scenes. On the synthetic datasets [14],

Table 1. Comparison with K -fixed methods on COCO [20], PASCAL VOC [11], and MOVi-C/E [14]. Results for SLATE, DINOSAUR, DINOSAUR-MLP, and SPOT are taken from SPOT [16]. Results for the remaining methods are taken from their original papers [12, 27]. Dashes indicate results not reported. The best values are in bold.

Method	Dec.	K -type	COCO			VOC			MOVi-C		MOVi-E	
			mBOc	mBOi	mIoU	mBOc	mBOi	mIoU	mBOi	mIoU	mBOi	mIoU
SLATE [25]	–	–	33.6	29.1	–	41.5	35.9	–	39.4	37.8	30.2	28.6
DINOSAUR [24]	Trans.	fixed	39.7	31.6	–	51.2	44.0	–	42.4	–	–	–
DINOSAUR-MLP [24]	MLP	fixed	30.9	27.7	–	40.9	39.5	–	39.1	–	35.5	–
SPOT [16]	Trans.	fixed	44.7	35.0	33.0	55.6	48.3	–	47.3	46.7	40.1	39.3
SPOT+FS+RC [27]	Trans.	fixed	45.3	35.7	–	56.5	49.3	–	49.0	47.8	–	–
DINOSAUR+FS+RC [27]	MLP	fixed	40.1	31.2	–	52.9	45.2	–	46.0	44.8	–	–
AdaSlot [27]	MLP	adaptive	–	27.4	–	–	–	–	35.6	–	29.8	–
MetaSlot [21]	MLP	adaptive	–	29.5	27.9	43.9	42.1	–	35.0	–	–	–
QASA	Trans.	adaptive	45.5	36.7	35.0	57.9	49.7	47.9	46.9	46.1	39.1	37.8
QASA-MLP	MLP	adaptive	36.5	33.6	32.5	53.8	47.3	45.5	42.2	41.1	34.6	33.0

Table 2. Comparison of K -adaptive methods on COCO [20], VOC [11] and MOVi-C/E [14]. The results for AdaSlot and MetaSlot are taken from the original paper [12, 21]. The best values are in bold.

Method	Dec.	K -type	mBOi			
			COCO	VOC	MOVi-C	MOVi-E
AdaSlot [27]	MLP	adaptive	27.4	–	35.6	29.8
MetaSlot [21]	MLP	adaptive	29.5	43.9	35.0	–
QASA	Trans.	adaptive	36.7	49.7	46.9	39.1
QASA-MLP	MLP	adaptive	33.6	47.3	42.2	34.6

our method likewise outperforms AdaSlot [12], as shown in Fig. 4, capturing sharper object boundaries rather than merely coarse blob-like outlines. The visualizations show that QASA learns slots that capture fine object details and bind more precisely to objects, while preserving the ability to adapt the number of objects per image.

To more directly illustrate the advantage of QASA, we further evaluate representative K -fixed methods (SPOT [16] and DINOSAUR [24]) on COCO under varying K (Fig. 1). As K changes, their performance fluctuates markedly. This sensitivity necessitates exhaustive per-dataset K sweeps, which are time- and compute-intensive, yet these sweeps still do not resolve the structural mismatch between a fixed slot budget and image-dependent object counts. Existing K -adaptive methods (AdaSlot [12] and MetaSlot [21]) can adaptively select the number of slots used per image, which saves substantial tuning effort and resources. However, they show a clear performance gap compared with K -fixed methods because they lack the slot-count prior. By contrast, QASA not only adaptively selects appropriate slots for each image for reconstruction, but also surpasses K -fixed methods in performance, thereby addressing the shortcoming of K -adaptive methods.

Comparison with K -fixed methods. Tab. 1 summarizes recent methods with fair comparability. The selected baselines include SLATE [25], DINOSAUR [24], SPOT [16], and +FS+RC [27]. Although we do not perform any per-dataset fine-tuning of K , QASA achieves *state-of-the-art* results on the real-world datasets COCO and VOC across all metrics. Unlike AdaSlot [12] and MetaSlot [21], whose strong results are largely limited to toy or synthetic settings, QASA surpasses K -fixed methods on real data and thereby offers clear practical benefits. We further compare QASA with K -fixed methods on synthetic datasets. Even without access to the hand-tuned prior of a fixed slot number, QASA attains *comparable* performance. For synthetic datasets, QASA performs slightly worse than the best K -fixed method when that method is evaluated at its optimal K . We hypothesize that object boundaries are clearer and object counts are explicit in synthetic data. Consequently, choosing an optimal K yields larger gains.

4.3. Ablation Study

Table 3. Influence of key components in Slot Selection. Coverage, Quality, and Novelty denote the corresponding mechanisms in the Quality-Guided Slot Selection. All results are evaluated on COCO [20]. The best values are in bold.

Coverage	Quality	Novelty	mBOc	mBOi	mIoU
×	×	×	25.9	25.5	24.9
✓	×	×	34.5	25.3	22.7
✓	✓	×	45.0	35.0	32.9
✓	✓	✓	45.5	36.7	35.0

For an in-depth analysis of the contributions of each component, we conduct several ablation studies. All ablations use the Transformer decoder. Unless otherwise specified, all hyperparameters remain unchanged.

Components of Quality-Guided Slot Selection. Starting from a model without gating, we progressively enable the components of the quality-guided slot selection (*coverage*, *quality*, and *novelty*), as shown in Tab. 3. Enabling *coverage* alone chiefly lifts mBOc but slightly harms mBOi and mIoU because diffuse/low-quality slots are admitted to meet the coverage target. Adding *quality* yields the largest jump overall by prioritizing high-quality slots, improving one-to-one alignment and boundary tightness. Incorporating *novelty* further gives a small gain on mBOc and clear gains on mBOi/mIoU by filtering overlapping slots.

Table 4. **Ablation on Gates in the Transformer decoder.** All results are evaluated on COCO [20]. The best values are in bold.

g_1	g_2	mBOc	mBOi	mIoU
\times	\times	25.9	25.5	24.9
\times	\checkmark	26.1	25.5	24.9
\checkmark	\times	43.1	33.2	30.9
\checkmark	\checkmark	45.5	36.7	35.0

Gates in the Transformer decoder. We further ablate the two-stage gating in the Gated Transformer Decoder, as reported in Tab. 4. Using only g_2 (logit gating) fails to enforce effective masking, likely because unattenuated logits can overwhelm the negative bias. Using only g_1 (key/value gating) already yields strong control, and combining g_1 with g_2 leads to additional gains. Concretely, g_1 scales the key and value vectors of unselected slots toward zero, which effectively shrinks their attention logits, while g_2 further adds a large negative bias to these logits, providing an extra margin that suppresses the influence of unselected slots.

Table 5. **Influence of the novelty threshold μ .** All results are evaluated on COCO [20].

Metric	novelty threshold μ					
	0	0.1	0.2	0.3	0.4	0.5
mBOc	45.0	45.5	45.8	45.5	45.5	45.6
mBOi	35.0	36.6	36.9	36.7	36.8	36.6
mIoU	32.9	34.9	35.2	35.0	35.2	34.9

Influence of the novelty threshold μ . Tab. 5 shows how mBOc, mBOi, and mIoU vary with the novelty threshold μ . Adding the novelty criterion clearly improves performance, especially for mIoU, and the strategy is robust, providing stable gains across a wide range of μ . Notably, we fix $\mu = 0.3$ in all experiments without tuning, which is sufficient to demonstrate the advantages of QASA.

Choice of K_{\max} . Unlike K -fixed methods that require searching for an optimal K , K -adaptive methods only specify K_{\max} and adaptively select effective slots per image.

Table 6. Effect of K_{\max} on MOVi-C and MOVi-E [14].

MOVi-C			MOVi-E		
K_{\max}	mBOi	mIoU	K_{\max}	mBOi	mIoU
15	44.4	43.4	24	38.3	36.8
18	46.5	45.7	28	39.1	37.8
20	46.9	46.1	30	39.1	37.8
22	46.4	45.6	32	39.3	38.0
24	46.3	45.7	34	39.5	38.3
32	45.4	45.0	64	38.7	38.3

In practice, setting K_{\max} to the maximum number of objects plus one (for background) usually works well. However, on the synthetic datasets MOVi-C and MOVi-E, we observe that moderately increasing K_{\max} can yield better results, as shown in Tab. 6. The gains from such slot redundancy are noticeably smaller on MOVi-E than on MOVi-C. We hypothesize this is because synthetic backgrounds are highly homogeneous, causing several slots to specialize to a few background modes. Increasing the number of redundant slots therefore helps. Since MOVi-E has more complex backgrounds than MOVi-C, this effect is reduced. Importantly, even without such redundancy ($K_{\max}=15$ for MOVi-C and $K_{\max}=24$ for MOVi-E), QASA still performs strongly. The table also shows that QASA is highly robust to the choice of K_{\max} : performance remains stable over a wide range, and even when K_{\max} is set far beyond the maximum object count ($K_{\max}=32$ for MOVi-C and $K_{\max}=64$ for MOVi-E), the degradation is minor, further supporting the effectiveness of the proposed K -adaptive mechanism.

5. Conclusion

We introduce a *Slot-Quality* metric that drives slots toward fine, object-specific features. Building on this metric, we present QASA, a K -adaptive Slot Attention method that selects the appropriate slots *per image*, better handling uncertainty in object cardinality. We decouple slot selection from decoding, removing the conflict between slot-count regularization and reconstruction. The framework supports both Transformer and MLP decoders. Empirically, QASA markedly outperforms existing K -adaptive methods by up to 8.4% on average. Without hand-tuning the optimal K , QASA achieves state-of-the-art performance on real-world datasets, outperforming K -fixed methods. While it is slightly weaker than K -fixed methods on synthetic datasets, where object boundaries are clearer and the optimal K provides a stronger prior, real-world scenarios are the true open sea for OCL. With a simple architecture, QASA closes much of the gap to K -fixed methods, further highlighting the promise of K -adaptive OCL.

References

- [1] Rim Assouel, Pau Rodriguez, Perouz Taslakian, David Vazquez, and Yoshua Bengio. Object-centric compositional imagination for visual abstract reasoning. In *ICLR 2022 Workshop on the Elements of Reasoning: Objects, Structure and Causality*, 2022. 1
- [2] Ondrej Biza, Robert Platt, Jan-Willem van de Meent, Lawson LS Wong, and Thomas Kipf. Binding actions to objects in world models. In *ICLR 2022 Workshop on the Elements of Reasoning: Objects, Structure and Causality*, 2022. 1
- [3] Christopher P Burgess, Loic Matthey, Nicholas Watters, Rishabh Kabra, Irina Higgins, Matt Botvinick, and Alexander Lerchner. Monet: Unsupervised scene decomposition and representation. *arXiv preprint arXiv:1901.11390*, 2019. 2
- [4] Mathilde Caron, Hugo Touvron, Ishan Misra, Hervé Jégou, Julien Mairal, Piotr Bojanowski, and Armand Joulin. Emerging properties in self-supervised vision transformers. In *ICCV*, pages 9650–9660, 2021. 3
- [5] Eric Crawford and Joelle Pineau. Spatially invariant unsupervised object detection with convolutional neural networks. In *AAAI*, pages 3412–3420, 2019. 2
- [6] Andrea Dittadi, Samuele Papa, Michele De Vita, Bernhard Schölkopf, Ole Winther, and Francesco Locatello. Generalization and robustness implications in object-centric learning. *ICML*, 2022. 1
- [7] Gamaleldin Elsayed, Aravindh Mahendran, Sjoerd Van Steenkiste, Klaus Greff, Michael C Mozer, and Thomas Kipf. Savi++: Towards end-to-end object-centric learning from real-world videos. *NIPS*, 35:28940–28954, 2022. 2
- [8] Martin Engelcke, Adam R Kosiorek, Oiwi Parker Jones, and Ingmar Posner. Genesis: Generative scene inference and sampling with object-centric latent representations. *ICLR*, 2020. 2
- [9] Martin Engelcke, Oiwi Parker Jones, and Ingmar Posner. Genesis-v2: Inferring unordered object representations without iterative refinement. *NIPS*, 34:8085–8094, 2021. 2
- [10] SM Eslami, Nicolas Heess, Theophane Weber, Yuval Tassa, David Szepesvari, Geoffrey E Hinton, et al. Attend, infer, repeat: Fast scene understanding with generative models. *NIPS*, 29, 2016. 2
- [11] Mark Everingham and John Winn. The pascal visual object classes challenge 2012 (voc2012) development kit. *PASCAL*, 8(5):2–5, 2011. 2, 5, 7
- [12] Ke Fan, Zechen Bai, Tianjun Xiao, Tong He, Max Horn, Yanwei Fu, Francesco Locatello, and Zheng Zhang. Adaptive slot attention: Object discovery with dynamic slot number. In *CVPR*, pages 23062–23071, 2024. 1, 2, 3, 5, 6, 7
- [13] Klaus Greff, Raphaël Lopez Kaufman, Rishabh Kabra, Nick Watters, Christopher Burgess, Daniel Zoran, Loic Matthey, Matthew Botvinick, and Alexander Lerchner. Multi-object representation learning with iterative variational inference. In *ICML*, pages 2424–2433. PMLR, 2019. 2
- [14] Klaus Greff, Francois Belletti, Lucas Beyer, Carl Doersch, Yilun Du, Daniel Duckworth, David J Fleet, Dan Gnanaprasam, Florian Golemo, Charles Herrmann, et al. Kubric: A scalable dataset generator. In *CVPR*, pages 3749–3761, 2022. 2, 5, 6, 7, 8
- [15] Jindong Jiang, Fei Deng, Gautam Singh, and Sungjin Ahn. Object-centric slot diffusion. In *NIPS*, 2023. 2
- [16] Ioannis Kakogeorgiou, Spyros Gidaris, Konstantinos Karantzalos, and Nikos Komodakis. Spot: Self-training with patch-order permutation for object-centric learning with autoregressive transformers. In *CVPR*, pages 22776–22786, 2024. 1, 2, 3, 4, 5, 6, 7
- [17] Thomas Kipf, Gamaleldin Fathy Elsayed, Aravindh Mahendran, Austin Stone, Sara Sabour, Georg Heigold, Rico Jonschkowski, Alexey Dosovitskiy, and Klaus Greff. Conditional object-centric learning from video. In *ICLR*, 2022. 2
- [18] Avinash Kori, Francesco Locatello, Fabio De Sousa Ribeiro, Francesca Toni, and Ben Glocker. Grounded object-centric learning. In *ICLR*, 2024. 2, 3, 6
- [19] Adam Kosiorek, Hyunjik Kim, Yee Whye Teh, and Ingmar Posner. Sequential attend, infer, repeat: Generative modelling of moving objects. *NIPS*, 31, 2018. 2
- [20] Tsung-Yi Lin, Michael Maire, Serge Belongie, James Hays, Pietro Perona, Deva Ramanan, Piotr Dollár, and C Lawrence Zitnick. Microsoft coco: Common objects in context. In *ECCV*, pages 740–755, 2014. 1, 2, 5, 7, 8
- [21] Hongjia Liu, Rongzhen Zhao, Haohan Chen, and Joni Paajarinen. Metaslot: Break through the fixed number of slots in object-centric learning. *NIPS*, 2025. 1, 2, 3, 6, 7
- [22] Francesco Locatello, Dirk Weissenborn, Thomas Unterthiner, Aravindh Mahendran, Georg Heigold, Jakob Uszkoreit, Alexey Dosovitskiy, and Thomas Kipf. Object-centric learning with slot attention. *NIPS*, 33:11525–11538, 2020. 1, 2
- [23] Davide Mambelli, Frederik Träuble, Stefan Bauer, Bernhard Schölkopf, and Francesco Locatello. Compositional multi-object reinforcement learning with linear relation networks. In *ICLR 2022 Workshop on Generalizable Policy Learning in Physical World*, 2022. 1
- [24] Maximilian Seitzer, Max Horn, Andrii Zadaianchuk, Dominik Zietlow, Tianjun Xiao, Carl-Johann Simon-Gabriel, Tong He, Zheng Zhang, Bernhard Schölkopf, Thomas Brox, et al. Bridging the gap to real-world object-centric learning. In *ICLR*, 2023. 1, 2, 3, 4, 5, 7
- [25] Gautam Singh, Sungjin Ahn, and Fei Deng. Illiterate dall-e learns to compose. In *ICLR*, 2022. 2, 7
- [26] Krishnakant Singh, Simone Schaub-Meyer, and Stefan Roth. Glass: Guided latent slot diffusion for object-centric learning. In *CVPR*, pages 28673–28683, 2025. 1
- [27] Pinzhuo Tian, Shengjie Yang, Hang Yu, and Alex Kot. Pay attention to the foreground in object-centric learning. In *CVPR*, pages 30281–30290, 2025. 1, 5, 7
- [28] Ziyi Wu, Jingyu Hu, Wuyue Lu, Igor Gilitschenski, and Animesh Garg. Slotdiffusion: Object-centric generative modeling with diffusion models. *NIPS*, 36:50932–50958, 2023. 2
- [29] Andrii Zadaianchuk, Maximilian Seitzer, and Georg Martius. Self-supervised visual reinforcement learning with object-centric representations. In *ICLR*, 2021. 1

- [30] Andrii Zadaianchuk, Maximilian Seitzer, and Georg Martius. Object-centric learning for real-world videos by predicting temporal feature similarities. *NIPS*, 36:61514–61545, 2023. [2](#)
- [31] Rongzhen Zhao, Huijing Wang, Juho Kannala, and Joni Pajarin. Multi-scale fusion for object representation. In *ICLR*, 2025. [1](#)